American Journal of Applied Sciences, 10 (3): 280-293, 2013
ISSN: 1546-9239

doi:10.3844/ajassp.2013.280.293 Published Online 10 (3) 2013 (http://www.thescipub.com/ajas.toc)

An Edge Detection Model Based on Virtual Magnetic Field: Application to Digital Color Images

[1.2]Nsiri, B. and [3]B. Bouda

[1]LIAD Laboratory,
[2]LPMMAT Laboratory,
Faculty of Sciences, Hassan II University, Casablanca, Morocco
[3]Department of Informatics, Faculty of Sciences and Technology, Moulay Ismail University, Errachidia, Morocco

Received 2012-07-03, Revised 2012-08-23; Accepted 2013-04-22

ABSTRACT

In computer vision, the edge detection is an essential and difficult problem to study. For this reason, many detectors were developed for gray-level and color images. However, these edge detectors may miss some parts of the edges. In the aim, to deal with this problem, a new approach is proposed. It is based on Virtual Magnetic Field (VMF) in conjunction with Cubical Voxels (CV). The main idea of this approach is to model a color image as a magnetic cube which has the same height and width as the image. The pixels intensities are modeled by the CV model as voxels that are considered by the VMF model as virtual magnetic moments. This technique allows determining easily the most important three operators that are used to provide approximate gradients for each plane color component. The method is tested on synthesized and real images that show promising results.

Keywords: Gray-Level and Color Images, Edge Detection, Gradient, Voxels, Magnetic Fiaeld

1. INTRODUCTION

Edges are locals, significant and detectable parts of images. Edge detection is highly crucial for many fields of computer vision such as object recognition and tracking, image retrieval, stereo vision and registration. Several edge detection algorithms are well-known and used by the computer vision community.

Gradient operators are commonly used to detect edges which are the abrupt changes of gray-level values in digital images. A gradient operator consists in two partial derivatives, which determine the magnitude and the direction of the gradient. Since a digital image is represented by a discrete function, the partial derivatives can only be approximated. Generally, the partial derivatives are implemented as a pair of convolution masks. As introduced in (Gonzalez and Woods, 2002), commonly used gradient operators include Prewitt (1970) and Sobel (1990) operator for horizontal and vertical edges, consisting of the partial derivative masks. This method basically uses the designed mask to traverse the image and detect edges by locating the maximum of the gradient'smagnitude in the considered image. However, this method is sensitive to noises, principally if the image is not smoothed. Canny (1986) uses three-steps algorithm to detect edges. At the first step, the original image is smoothed by convolving a two dimensional Gaaussian function with a proper variance. At the second step, masks detecting the horizontal, vertical and sometimes the diagonal edges are used to compute the gradient of the smoothed image. Edges are then traced at the third stage. The Canny edge detection algorithm (Canny, 1986) needs to adjust two thresholds and a standard deviation of Gaussian smooth mask to yield a proper result. For practical applications, edge detection is only the first step in image analysis, consequently, should be short as possible. Some complicated edge detectors are not used in practice

Corresponding Author: Nsiri, B., LIAD Laboratory, Faculty of Sciences, Hassan II University, Casablanca, Morocco

despite having good quality. Edge detection is a critical element in image processing since edges contain a major function of image information. The function of edge detection is to identify the boundaries of homogeneous regions in an image based on properties such as intensity and texture.

In the last decade, color information has received attention from the scientific community for detecting edges (Koschan, 1995; Roman *et al*., 1995; Economou *et al*., 2001; Koschan and Abidi, 2005; Zaart, 2010). Color images provide more information than gray-level images. It has been shown that the result of edge detection is improved by about 10% when using color image instead of gray-level one (Novak and Shafer, 1987). The difficulty in extending derivative approaches to color images arises from the fact that the image function is vector-valued. Whenever the gradients of image components are computed, the question remains of how to combine them onto one result. For the solution of this problem, three techniques are used. In traditional gray-value technique, a color image is converted to a gray-level one and then information is treated in the gray-level image. Monochromatic-based techniques consist in existing information from the individual color channels or color vector components, then combining the obtained individual results. Vector-valued techniques treat the color information as color vectors in a vector space provided with a vector norm. Generally, the traditional technique show better results than standard ones. These techniques have been applied by Koschan (1995) to the three coalor channels and performed a comparative study on color edge detection. Compared with Monochromatic based techniques, vector-valued techniques are new and give better results. Cumani (1991) described a method based on the second-order derivatives to detect edges in color and multispectral images. Koschan and Abidi (2005) made another contribution on vector-valued techniques and demonstrate that better results are achieved with the Cumani (1991). Novak and Shafer (1987) and Kanade *et al*. (1989) extended a Canny (1986) to color images. Robinson (1977) and Ruzon and Tomasi (1999) applied compass edge detectors to color images. Djuric and Fwu (1997) used the maximum a posteriori criterion based on Bayesian theory to locate and detect edges in vector images. Evans and Liu (2006) described a color morphological gradient operator based on vector differences to detect edges in multivariate images. Weijer *et al*. (2005) proposed a new type of edge detector by photometric quasi-invariants. Weijer *et al*. (2006) proposed another approach based on photometric invariance theory and tensor to get a robust color edge detector, while, Bouda *et al*. (2008) developed edge detection in color images based on virtual electric field model.

One of the main challenges to color edge detection is how to compute the gradients for each plane component by an appropriate operator. A default method is to use the same horizontal and vertical mask for the different color components. Unfortunately, the summation of the gradients computed is often inadequate and result in a loss of color information. This naive method ignores completely the strong correlation between the different components of the color image. To avoid the above problem and to recuperate this loss color information, we propose an edge detection operator based on Virtual Magnetic Field (VMF). The new method Virtual Magnetic Field Model (VMFM) allows us to design two relative masks for each color component. The image intensities are modeled as voxels and each voxel is considered as a magnetic moment. The magnetic forces between the central moment and its neighborhoods allow us to determine the masks relative to each color component. These masks are useful to approximate gradients by a simple convolution operation with image components. The last stage is to combine the result by using the color gradients in the image vectors. This method has been proposed in the color edge detection in numerous referenced articles (Novak and Shafer, 1987; Bouda *et al*., 2008; Zenzo, 1986; Lee and Cok, 1991).

1.1. Fuandamental Tools

1.1.1. Tiling and its Associated Mesh

In two dimensions, a tiling of the plane is defined as a partition of an infinite plane onto disjoined cells. When the same geometrical configuration is used to make the partition, a tiling is called regular. The main idea in image processing is the repetitiveness in the infinity and the regular juxtaposition of geometrical configurations (Borgefors, 1984; Chassery and Montanvert, 1991). The three most used tilings of the plane are square, triangular and hexagonal ones. Square, hexagonal and triangular tilings are respectively associated square, triangular and hexagonal meshes. Square mesh is the more used theme in image processing for two reasons. The first one is relative to the constraint technological imposed by industry. The second one is that the square mesh allows to structure data in a traditional matrix form (**Fig. 1**). Pixels in three dimensions are known as voxel. Like the plane, the partition of the space in voxels can also be represented by a tiling. Thus, it is interesting for color images to use a tiling of the cube, to which corresponds a cubical mesh. A set of these meshes forms voxels. These last ones are represented by their three coordinates (**Fig. 2**).

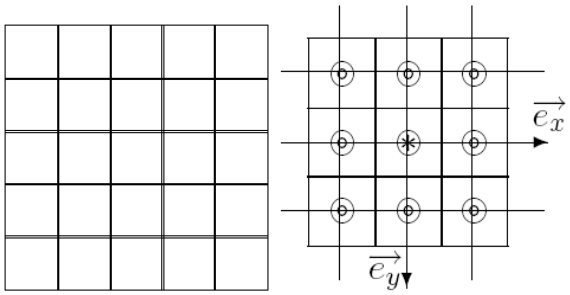

Fig. 1. Tiling of the plane and its associated mesh

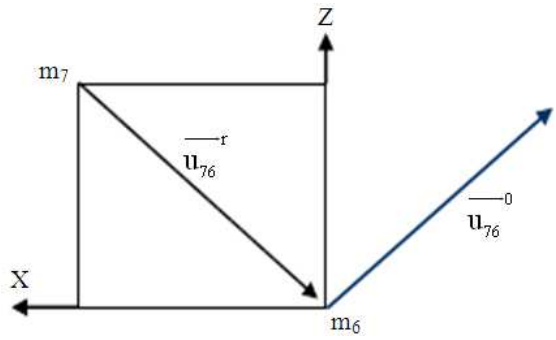

Fig. 2. $\vec{u}_{ij}^{r}$ and $\vec{u}_{ij}^{\theta}$ representation (example $\vec{u}_{76}^{r}$, $\vec{u}_{76}^{\theta}$)

1.2. Magnetic Field

It is well known that the electric current exerts the magnetic field, which is described by the Biot-Savart law. The magnetic field lines are generated by a current carrying wire form concentric circles around the wire. The direction loop of this field is determined by the right hand grip rule. Moreover, the strength of the magnetic field decreases with the distance rfrom the wire. Considering a magnetic moment mplaced at point p(p_r, p_θ, p_z) (**Fig. 3**), the moment generates an magnetic field $\vec{B}$ at point p(p_r, p_θ, p_z) in the cylindrical coordinates $\left(o,\vec{e}_r,\vec{e}_\theta,\vec{e}_z\right)$ (**Fig. 3**). The magnetic field created by the magnetic moment m, due to the electric current, is equal to Equation 1:

$$\vec{B} = \frac{m\mu o}{4\pi}\begin{vmatrix} \frac{2\cos(\theta)}{r^3} \\ \frac{\sin(\theta)}{r^3} \\ 0 \end{vmatrix} \quad (1)$$

Where ris the distance between the moment and the centerμ_0 is the per meability of free space

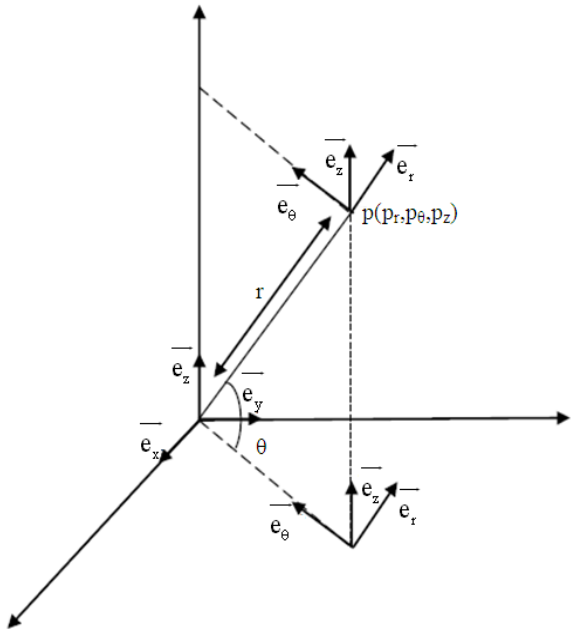

Fig. 3. Cylindrical coordinates

2. MATERIALS AND METHODS

2.1. Virtual Magnetic Field Model (VMFM)

Based on the above description, the color image I is proposed to be modeled as a network of cubical voxels of virtual magnetic moments. The CV model describes the color pixel as a cubical voxel. Hence, each block of 3×3 pixels of the color image is modeled as an elementary cube. The VMF model describes the voxels as punctual magnetic moments uniformly distributed on the cube (**Fig. 4a**). A set of elementary cubes forms a color image as shown in **Fig. 4b**. Regarding one elementary cube, the central cubical voxel and its neighbors m_i (i = 1,…,12) are distributed with respect to diagonal neighbors distribution. The elementary cube has sides a, diagonal $a\sqrt{3}$ and its faces are perpendicular to the coordinate axes in the coordinate space $\left(o,\vec{e}_x,\vec{e}_y,\vec{e}_z\right)$.

As shown in **Fig. 5**, a voxel has 26 neighbors. Moreover, there are three kinds of distributions: diametric neighbor voxels (according to the directions of the cubes' diameters), axial neighbor voxels (according to the axes) and diagonal neighbor voxels (according to the diagonals in 3 orthogonal planes).

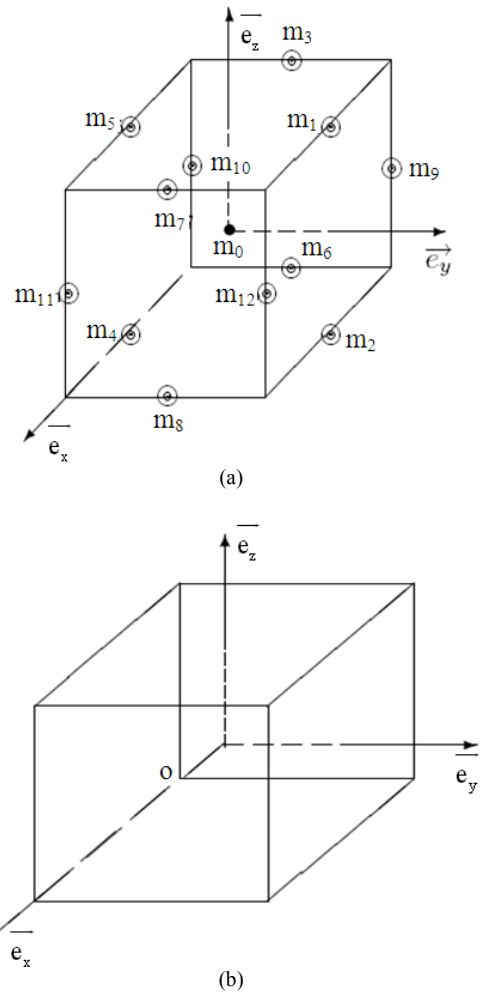

Fig. 4. Proposed CVMFM for a color image: (a) the VMF model for one elementary cube of the color image; (b) the CV model for a colorimage

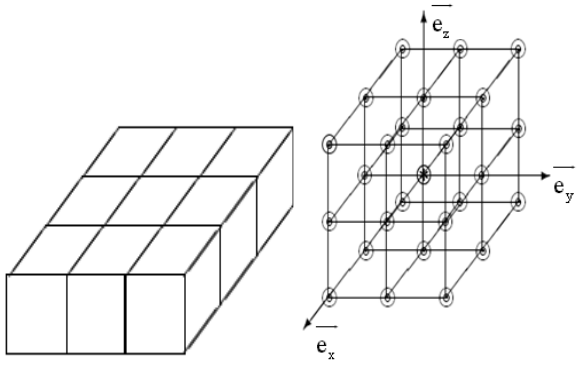

Fig. 5. Tiling of the cube and its associated mesh

As represented in **Fig. 4a**, in the proposed approach, we consider cubical voxels with a virtual model of magnetic moments m_i, where $i \in \{1,\ldots,12$ Each moment m_i creates, in the center m_0 of the cubical voxels, a virtual magnetic field $\vec{B}_{mi/m_0}$. The unity vector between m_i and m_j for $j \in \{1,\ldots,12$ is noted by $\vec{u}_{ij}^{r} = \frac{\overline{m_i m_j}}{\| m_i m_j \|}$, where $\vec{u}_{ij}^{\theta}$ and $\vec{u}_{ij}^{r}$ are orthogonal. **Figure 2** illustrates an example of the unity vector $\vec{u}_{76}^{r}$.

From this figure, we remark that the angle between the vector $\vec{u}_{76}^{r}$ and the axes x and z is equal to -π/4. $\vec{u}_{76}^{r} = -\cos\left(\frac{-\pi}{4}\right)\vec{e}_x - \cos\left(\frac{-\pi}{4}\right)\vec{e}_z = -\frac{\sqrt{2}}{2}\left(\vec{e}_x + \vec{e}_z\right)$, and $\vec{u}_{76}^{\theta} = -\cos\left(\frac{-\pi}{4}\right)\vec{e}_x + \cos\left(\frac{-\pi}{4}\right)\vec{e}_z = -\frac{\sqrt{2}}{2}\left(\vec{e}_x - \vec{e}_z\right)$ For example, we calculate the magnetic fields $\vec{B}_{m_6/m_0}, \vec{B}_{m_7/m_0}$ as fellow Equation 2 and 3:

$$\vec{B}_{m_6/m_o} = -\frac{K}{r^3} 2m_6 \left(2\cos(\theta)\vec{u}_{7,6}^{r} + \sin(\theta)\vec{u}_{7,6}^{\theta}\right) \quad (2)$$

$$\vec{B}_{m_7/m_o} = -\frac{K}{r^3} 2m_7 \left(2\cos(\theta)\vec{u}_{7,6}^{r} + \sin(\theta)\vec{u}_{7,6}^{\theta}\right) \quad (3)$$

Where,

$\vec{u}_{7,6}^{\theta} = \frac{\sqrt{2}}{2}\left(-\vec{e}_x + \vec{e}_z\right), \vec{u}_{7,6}^{r} = -\frac{\sqrt{2}}{2}\left(\vec{e}_x + \vec{e}_z\right), K = \frac{\mu_0}{8\pi}, \theta = \frac{\pi}{2}$ and ris the distance between the moment and the center. In the approach proposed, we consider that the virtual magnetic moments correspond to the gray-levels of voxels. Hence, the central cubical voxel is subjected to the magnetic of the 12 neighboring charges. To see how to use Equation 1 and 2 to calculate the magnetic field for a set of moment magnetic cubical, we suppose that virtual moment m_i, $i \in \{1,\ldots,12$, are diametrically opposed in the cube. The magnetic fields, where the virtual moments m_i (i = 1,…,12) are diametrically opposed, are given respectively by the following Equation 4-9:

$$\vec{B}_{m_7/m_6} = \vec{B}_{m_7/m_0} + \vec{B}_{m_6/m_0} = \frac{K}{r^3}\left(2m_7 - 2m_6\right)\vec{u}_{7,6}^{\theta} \quad (4)$$

$$\vec{B}_{m_4/m_1} = \vec{B}_{m_4/m_0} + \vec{B}_{m_1/m_0} = \frac{K}{r^3}\left(2m_4 - 2m_1\right)\vec{u}_{4,1}^{\theta} \quad (5)$$

$$\vec{B}_{m_5/m_2} = \vec{B}_{m_5/m_0} + \vec{B}_{m_2/m_0} = \frac{K}{r^3}\left(2m_5 - 2m_2\right)\vec{u}_{5,2}^{\theta} \quad (6)$$

$$\vec{B}_{m_8/m_3} = \vec{B}_{m_8/m_0} + \vec{B}_{m_3/m_0} = \frac{K}{r^3}\left(2m_8 - 2m_3\right)\vec{u}^{\theta}_{8,3} \quad (7)$$

$$\vec{B}_{m_{10}/m_{12}} = \vec{B}_{m_{10}/m_0} + \vec{B}_{m_{12}/m_0} = \frac{K}{r^3}\left(2m_{10} - 2m_{12}\right)\vec{u}^{\theta}_{10,12} \quad (8)$$

$$\vec{B}_{m_{11}/m_9} = \vec{B}_{m_{11}/m_0} + \vec{B}_{m_9/m_0} = \frac{K}{r^3}\left(2m_{11} - 2m_9\right)\vec{u}^{\theta}_{11,9} \quad (9)$$

The unitary vectors $\overrightarrow{U_{7,6}}, \overrightarrow{U_{4,1}}, \overrightarrow{U_{5,2}}, \overrightarrow{U_{8,3}} \overrightarrow{U_{10,12}}$ and $\overrightarrow{U_{11,9}}$ can be concisely represented as a function of $\vec{e}_x, \vec{e}_y$ and $\vec{e}_z$, in the Cartesian coordinate space $\left(o, \vec{e}_x, \vec{e}_y, \vec{e}_z\right)$. The **Fig. 6a** illustrates a distribution of $p_j$points in the cube ofsides a. Two elementary cubes of sides a = 2 of this figure are depicted in **Fig. 6b and 6c**.

Let $\vec{U}^r_{7,6} = \vec{U}^r_{7,0} = -\vec{U}^r_{6,0}$ be the unitary vector, where $\vec{U}^r_{6,0} = \cos\left(\overrightarrow{U^r_{6,0}}, \vec{e}_x\right)\vec{e}_x + \cos\left(\overrightarrow{U^r_{6,0}}, \vec{e}_z\right)\vec{e}_z$. Based on the depicted elementary cube in **Fig. 6b** and the rectangle ($p_0p_{16}p_6p_{17}$), the angles $p_0\hat{p}_6p_{17} = p_0\hat{p}_6p_{16} = \frac{\pi}{4}$. As result, $\vec{U}^r_{6,0} = \frac{\sqrt{2}}{2}\left(\vec{e}_x + \vec{e}_z\right)$. Consequently, $\vec{U}^r_{7,6} = \frac{\sqrt{2}}{2}\left(\vec{e}_x + \vec{e}_z\right)$.

By considering the elementary cube depicted in **Fig. 6c**, the unitary vector $\vec{U}^r_{4,1}$ can be easily determined. In this case, let $\vec{U}^r_{4,1} = \vec{U}^r_{4,0} - \vec{U}^r_{0,1}$, where $\vec{U}^r_{0,1} = \cos\left(\overrightarrow{U^r_{0,1}}, \vec{e}_y\right)\vec{e}_y + \cos\left(\overrightarrow{U^r_{0,1}}, \vec{e}_x\right)\vec{e}_z$. In the rectangle ($p_0p_{15}p_1p_{14}$), the angles $p_1\hat{p}_0p_{14} = p_1\hat{p}_0p_{15} = \frac{\pi}{4}$. Thus, we will have $\vec{U}_{0,1} = \frac{\sqrt{2}}{2}\left(\vec{e}_y + \vec{e}_z\right)$. Finally, we get $\vec{U}_{4,1} = \frac{\sqrt{2}}{2}\left(\vec{e}_y + \vec{e}_z\right)$.

Similarly and following the same development above, we find the four other vectors $\vec{u}^{\theta}_{4,1} = \frac{\sqrt{2}}{2}\left(-\vec{e}_y + \vec{e}_z\right), \vec{u}_{5,2} = \frac{\sqrt{2}}{2}\left(\vec{e}_y + \vec{e}_z\right), \vec{u}_{8,3} = \frac{\sqrt{2}}{2}\left(\vec{e}_x + \vec{e}_z\right)$, $\vec{u}^{\theta}_{11,9} = \frac{\sqrt{2}}{2}\left(-\vec{e}_x - \vec{e}_y\right)$ and $\vec{u}^{\theta}_{10,12} = \frac{\sqrt{2}}{2}\left(-\vec{e}_x + \vec{e}_y\right)$.

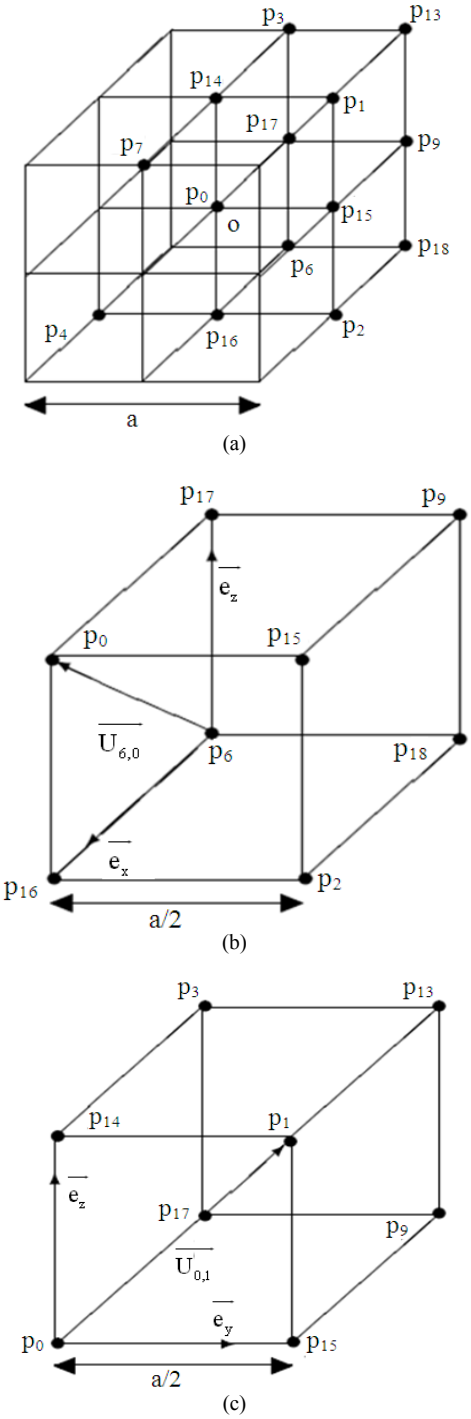

Fig. 6. The elementary cubes and the angles to determine the projection of the vectors $U^r_{7,6}$ and $U^r_{4,1}$ against e_x, e_z and e_z vectors

If n moment magnetic are presented, then the total magnetic field $\vec{B}_{tot}$ is given by the vector sum of each moment magnetic Equation 10:

$$\vec{B}_{tot} = \sum_{i=1}^{n} \vec{B}_i \quad (10)$$

When n = 12, the total magnetic field in the coordinate space $\left(o, \vec{e}_x, \vec{e}_y, \vec{e}_z\right)$ is given respectively by the following Equation (11-13):

$$\vec{B}_{e_x} = \frac{K}{r^3}\sqrt{2}\,(-m_3 + m_6 - m_7 + m_8 + m_9 - m_{10} - m_{11} + m_{12})\vec{e}_x, \quad (11)$$

$$\vec{B}_{e_y} = \frac{K}{r^3}\sqrt{2}\,(m_1 - m_2 - m_4 + m_5 + m_9 + m_{10} - m_{11} - m_{12})\vec{e}_y, \quad (12)$$

$$\vec{B}_{e_z} = \frac{K}{r^3}\sqrt{2}\,(-m_1 - m_2 - m_3 + m_4 + m_5 - m_6 + m_7 + m_8)\vec{e}_z, \quad (13)$$

In **Fig. 7**, we give the projections of charges mi shown in **Fig. 7a** onto planes $\prod_{xy} = \left(\vec{e}_x \text{ o } \vec{e}_y\right), \prod_{yz} = \left(\vec{e}_y \text{ o } \vec{e}_z\right)$ and $\prod_{zx} = \left(\vec{e}_z \text{ o } \vec{e}_x\right)$. Using Equation 12 and the matrix shown in **Fig. 7a**, we deduce the 3×3 mask hxa given in **Fig. 8a**. Similarly, with Equation 13 and the matrix shown in **Fig. 7b**, we obtain the mask hya depicted in **Fig. 8b**. Finally, from Equation 14 and the matrix shown in **Fig. 7c**, we deduce the mask hza depicted in **Fig. 8c**.

Figure 9 illustrates an example of gray-level and color image using VMFM method. The RGB original image is transformed to gray-level image by calculating the mean value over the three color components. The approximate gradients are obtained by convolution of each component with masks depicted in **Fig. 8** and their transposed masks. The norm of gradient is given by:

$$Grad = \sqrt{|Grad_R|^2\ Grad_G|^2 + |Grad_B|^2} \quad (14)$$

where, $Grad_R$, $Grad_G$and $Grad_B$are the gradients of red, green and blue components respectively. From these results, we note that some of the edges not determined in the gray-level image (**Fig. 9d**), could be detected in color image (**Fig. 9c**).

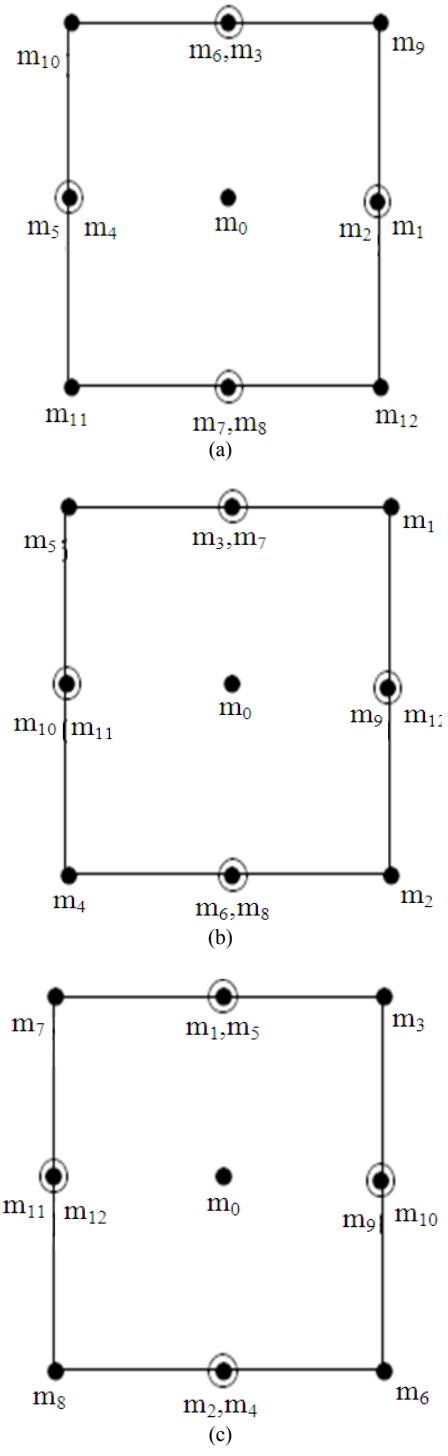

Fig. 7. The projection of onto planes: (a) $\prod_{xy}$ (b) $\prod_{yz}$ (c) $\prod_{zx}$

$-\sqrt{2}$	0	$\sqrt{2}$
0	0	0
$-\sqrt{2}$	0	$\sqrt{2}$

(a)

$\sqrt{2}$	0	$\sqrt{2}$
0	0	0
$-\sqrt{2}$	0	$-\sqrt{2}$

(b)

$\sqrt{2}$	0	$-\sqrt{2}$
0	0	0
$\sqrt{2}$	0	$-\sqrt{2}$

(c)

Fig. 8. The obtained 3×3 masks by VMFM. (a) h_{xa}, (b) h_{ya}, (c) h_{za}

(a)

(b)

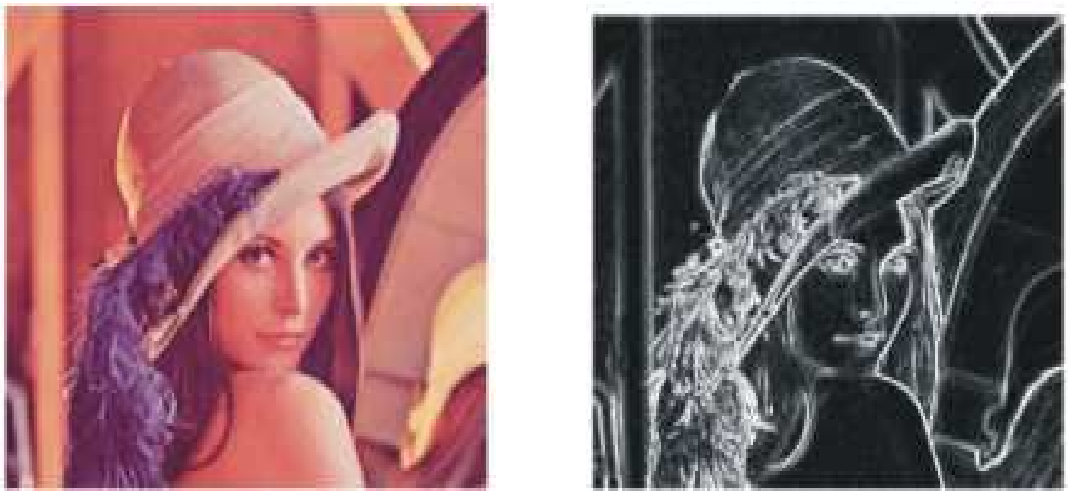

(c) (d)

Fig. 9. Results of gradient norm from the Lenna image. (a) Original RGB image; (b) gradient norm for acolor image based on VMFM; (c) gray-level representation; (d) gradient norm for a gray-level image based on VMFM.

2.2. Combination of Gradients

The approximate gradients for each image component provided by the first step (previous subsection) should be combined to obtain the resulting gradients. Various methods have been defined and used to combine gradients in color images (Cumani, 1991; Zenzo, 1986; Lee and Cok, 1991). Since the vector valued technique m:give the better results, we use this technique in the following.

Let $\Psi(u_1u_2):\Re^2\to\Re^m$ be a m-band image with components $\Psi(u_1u_2):\Re^2\to\Re, i=1,2,...,m$. In RGB mequal to 3 components. In the plane coordinates, we have u_i with i = 1,2. The more usual notation (x,y) is $u_1 \equiv x$ and $u_2 \equiv y$. The value of the image at a given point (u_1^0,u_2^0) is a vector in $\Re^m$. The difference of image values at two points $P=(u_1^0,u_2^0))$ and $Q=(u_1^1,u_2^1)$ is given by $\Delta\Psi=\Psi(P)-\Psi(Q)$. When the distance d(P,Q) between P and Q is infinite small displacement, the difference $d\Psi$ and its squared norm $d\Psi^2$ are given by Equation 15:

$$d\Psi=\sum_{i=1}^{2}\frac{\partial\Psi}{\partial u_i}du_i \tag{15}$$

$$d\Psi=\sum_{i=1}^{2}\sum_{j=1}^{2}\frac{\partial\Psi}{\partial u_i}\frac{\partial\Psi}{du_i}du_i\,du_j \tag{16}$$

The Equation (16) can be rewritten in quadratic form asdescribed by the following equation:

$$d\Psi^2=\begin{bmatrix}du_1\\du_2\end{bmatrix}^T\begin{bmatrix}g_{11}&g_{12}\\g_{12}&g_{22}\end{bmatrix}\begin{bmatrix}du_1\\du_2\end{bmatrix}, \tag{17}$$

where $g_{ij}=\frac{\partial\Psi}{\partial u_i}\frac{\partial\Psi}{\partial u_j}$.

The extrema of the Equation (17) are obtained by finding the directions of the $[g_{ij}]$ matrix eigenvectors. The obtained values are corresponding to the eigenvalues λ±and the eigenvectors η±given by Equation 18 and 19:

$$\lambda\pm=\frac{g_{11}+g_{22}}{2}\pm\sqrt{\frac{(g_{11}-g_{22})^2}{4}+g_{12}^2} \tag{18}$$

$$\eta_\pm=(\cos\theta\pm,\sin\theta\pm), \tag{19}$$

whereθ±are given (modulo π) by:

$$\begin{cases}\theta_+=\frac{1}{2}\arctan\left(\frac{2g_{12}}{g_{11}-g_{12}}\right)\\ \theta_-=\theta_++\frac{\pi}{2}\end{cases}$$

The eigenvectors provide the direction of maximal and minimal changes at a given point in the image. While, the corresponding eigenvalues represents the rate of each change. θ+ is called the direction of maximal change. While, $\lambda+$ is the maximal rate of change. Similarly, θ_- and λ_- are respectively the direction of minimal change and the minimal rate of change. A possible choice is the subtraction $f = f(\lambda_+ - \lambda_-)$ as proposed in (Cumani, 1991).

Based on the results and the ideas above, we suggest new color edge detection:

Since a function of the form $f = f(\lambda_+ - \lambda_-)$ is the analog multi-spectral extension of $f = f\left(\left\|\nabla\Psi\right\|^2\right)$ for monochromatic images m = 1, the image processing algorithms for mono-spectral images based on $\left\|\nabla\Psi\right\|^2$ can be extended to color images by replacing the squared magnitude of the gradient with Equation 20:

$$\left\|\nabla\Psi\right\| = \sqrt{\lambda_+ - \lambda_-} \tag{20}$$

Algorithm

The proposed algorithm to find edges is as follow:

Step 1: Describe each color image pixel as a cubical voxel by using the CV approach
Step 2: Describe each voxel as a magnetic moment by using the VMF model
Step 3: Calculate, for each plane component, the 3×3 mask according to the VMFM
Step 4: Compute the magnitude of the gradient

3. RESULTS AND DISCUSSION

Real and synthetic images are used to evaluate the performance of our algorithm in comprising with those of Cumani and Canny since they have given the best results in the literature. A global discussion of several criteria for the evaluation of edge detectors is given for gray-level images in (Salotti *et al*., 1996), while is given for gray-level and color images in (Koschan, 1995; Koschan and Abidi, 2005; Singh and Singh, 2008). **Figure 10** presentgood resultsby applying the norm of gradient VMFM to four synthetic and real color images:

- 256×256 synthetic image, which composed of five regions
- 300×300 synthetic Squares that contains four colors
- 303×250 real image
- 326×256 real Castle image

Figure 11 illustrates the original images used for evaluating our algorithm and the results. From this image we can seen that although the VMFM is computationally simpler, its performance is good for both synthetic and real images.

(a)

(b)

Fig. 10. Norm of gradient VMFM: (a,c,e,g) Original images; (b,d,f,h) Norm of VMFM gradient

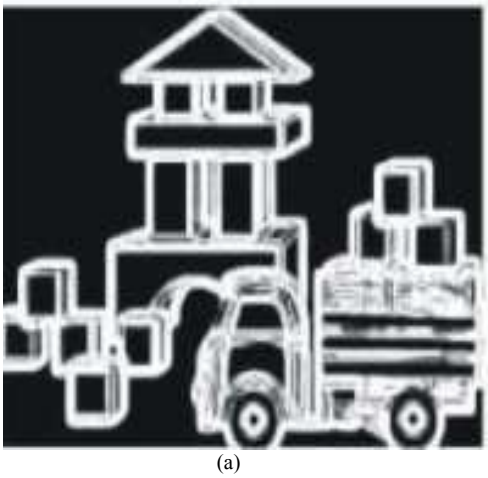

(a)

(b)

(c)

(d)

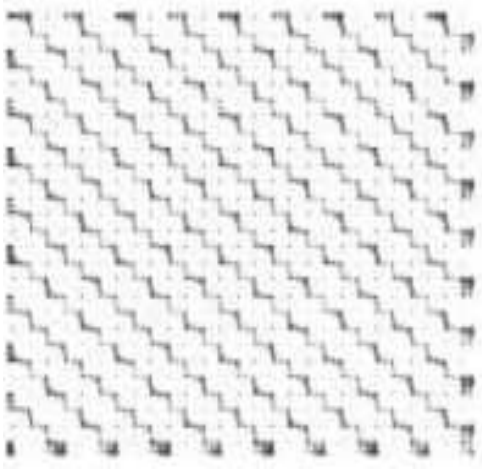

(e)

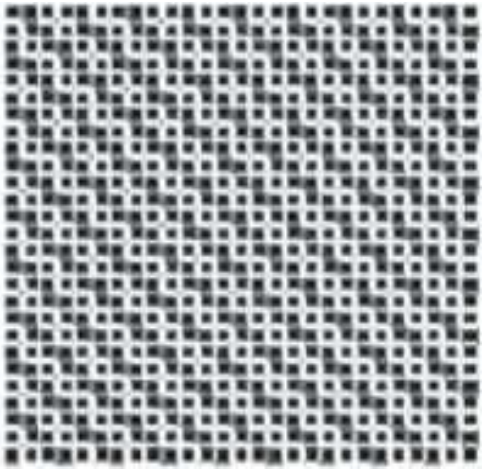

(f)

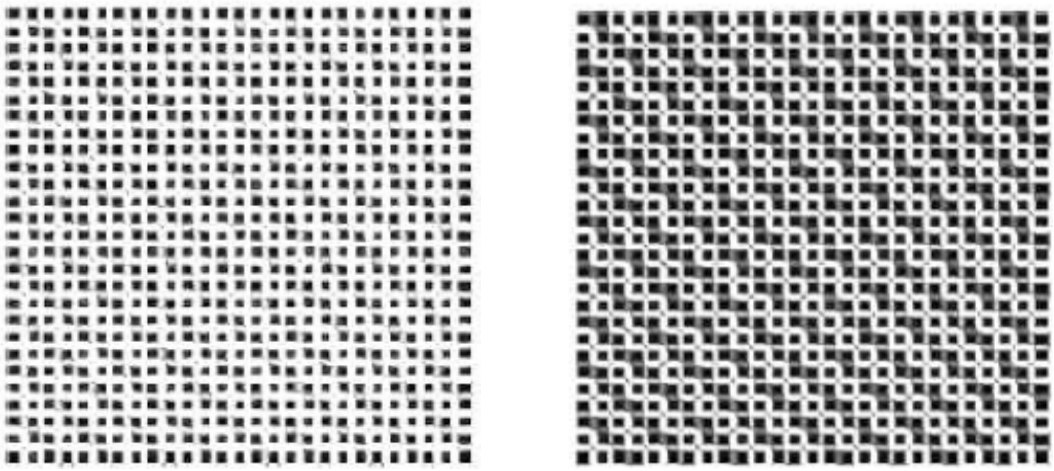

(g) (h)

Fig. 11. (a,e) Canny approach; (b,f) Cumani approach; (c,g) CVVEF approach; (d,h)VMFM approach

(a) (b)

(c) (d)

(e)

(f)

Fig. 12. Images of simulation. (a) Speelgoed1; (b) Squares; (c) Clown; (d) Speelgoed2; (e) Bloks; (f) Girl

To compare the performance of our approach to other ones, the color Canny and Cumany operators are tested with VMFM-based edge detector. To this end, seven images are used (**Fig. 12a-f)**:

- 300×300 blurred synthetic Squares
- 243×243 synthetic image containing three different color squares
- 512×512 real Tiffany
- 512×512 real Clown
- 720×576 real Barbara
- 256×256×3 speelgoed
- 288×360 soil data set images

The results can be interpreted as follows: from the obtained edges with the Canny operator (**Fig. 11a,e**), we remarked the non detection of some edges that are successfully detected with the Cumani operator (**Fig. 11b,f**) CVVEF (**Fig. 11c,g**) and the VMFM operator (**Fig. 11d,h**). Moreover, in addition to its simple characteristics, more edge results are achieved with the VMFM method. Furthermore, the computation complexity of this method is low. Known that the computation of the proposed approach is based on the convolution of the image and the filter coefficients in 3 spaces, we conclude that the computation complexity of this approach is equal to 3times the convolution complexity.

4. CONCLUSION

In this study, we have proposed a new approach (VMFM) for edge detection in color images. For each input image component, the VMFM's result is determined by a designed operator that ensures a good gradient estimation in color images. The operator results are attained without computational expense, since; they are given by the first-order of differential operators. Moreover, the experimental results in edge detection are very encouraging.

5. REFERENCES

Borgefors, G., 1984. Distance transformations in arbitrarydimensions. Comput. Vison Graph. Image Process., 27: 321-345. DOI: 10.1016/0734-189X(84)90035-5

Bouda, B., L. Masmoudi and D. Aboutajdine, 2008. CVVEFM: Cubical voxels and virtual electric field model for edge detection in color images. Signal Process., 88: 905-915. DOI: 10.1016/j.sigpro.2007.10.006

Canny, J., 1986. A computational approach to edge detection. IEEE Trans. Pattern Anal. Mach. Intell., 8: 679-698. DOI: 10.1109/TPAMI.1986.4767851

Chassery, J.M. and A. Montanvert, 1991. Montanvert, Geometrie discrete en analyse d'images. Hermes, Paris.

Cumani, A., 1991. Edge detection in multispectral images. CVGIP: Graph. Mod. Image Process., 53: 40-51. DOI: 10.1016/1049-9652(91)90018-F

Djuric, P.M. and J.K. Fwu, 1997. On the detection of edges in vector images. IEEE Trans. Image Process., 6: 1595-1601. DOI: 10.1109/83.641421

Economou, G., A. Fotinos, S. Makrogiannis and S. Fotopoulos, 2001. Color image edge detection based on nonparametric density estimation. Proceedings of the International Conference on Image Processing, Oct. 07-10, IEEE Xplore Press, Thessaloniki, pp: 922-925. DOI: 10.1109/ICIP.2001.959197

Evans, A.N. and X.U. Liu, 2006. A morphological gradient approach to color edge detection. IEEE Trans. Image Process., 15: 1454-1463. DOI: 10.1109/TIP.2005.864164

Gonzalez, R.C. and R.E. Woods, 2002. Digital Image Processing. 2nd Edn., Prentice Hall, Upper Saddle River, NJ., ISBN-10: 0201180758, pp: 793.

Kanade, T. and S. Shafer, 1989. Image understanding research at Carnegie Mellon. Proceedings of the workshop on Image Understanding Workshop, (IUW '89), Morgan Kaufmann Publishers Inc. San Francisco, CA, USA., pp: 32-48.

Koschan, A. and M. Abidi, 2005. Detection and classification of edges in color images. IEEE Signal Process. Mag., 22: 64-73. DOI: 10.1109/MSP.2005.1407716

Koschan, A., 1995. A comparative study on color edge detection. Proceedings 2nd Asian Conference on Computer Vision, Dec. 5-8, Singapore, pp: 574-578.

Lee, H.C. and D.R. Cok, 1991. Detecting boundaries in a vector field. IEEE Trans. Signal Process., 39: 1181-1194. DOI: 10.1109/78.80971

Novak, C.L. and S.A. Shafer, 1987. Color edge detection. Proceedings of the DARPA Image Understanding Workshop, (IUW' 87), Los Angeles, CA, USA., pp: 35-37.

Prewitt, J.G., 1970. Object Enhancement and Extraction. In: Picture Processing and Psychopictorics, Lipkin, B.S. and A. Rosenfeld (Eds.), Academic Press, New York, pp: 75-149.

Robinson, G.S., 1977. Color edge detection. Opt. Eng., 16: 165479-165479. DOI: 10.1117/12.7972120

Roman, P., R. Klette, A. Koschan and T. Kuchynsky, 1995. A fast algorithm for edge structure detection in monochrome and color images. Mach. Graph. Vis., 4: 59-77.

Ruzon, M.A. and C. Tomasi, 1999. Color edge detection with the compass operator. Proceedings of the IEEE Computer Society Conference on Computer Vision and Pattern Recognition, Jun. 23-25, IEEE Xplore Press, Fort Collins, CO. DOI: 10.1109/CVPR.1999.784624

Salotti, M., F. Bellet and C. Garbay, 1996. Evaluation of edge detectors: Critics and proposal. Proceedings of the Workshop Performance Characteristics Vision Algorithms, (CVA' 96), pp: 81-97.

Singh, B. and A.P. Singh, 2008. Edge detection in gray level images based on the shannon entropy. J. Comput. Sci., 4: 186-191.

Sobel, I., 1990. An Isotropic Image Gradient Operator. In: Machine Vision for Three-Dimensional Scenes, Freeman, H. (Ed.), Academic Press, Boston, ISBN-10: 0122667220, pp: 376-379.

Weijer, J.V.D., T. Gevers and J.M. Geusebroek, 2005. Edge and corner detection by photometric quasi-invariants. IEEE Trans. Patt. Anal. Mach. Intell., 27: 625-630. DOI: 10.1109/TPAMI.2005.75

Weijer, J.V.D., T. Gevers, A. Smeulders, 2006. Robust photometric invariant features from the color tensor. IEEE Trans. Image Process., 15: 118-127. DOI: 10.1109/TIP.2005.860343

Zaart, A.E., 2010. A novel method for edge detection using 2 dimensional gamma distribution. J. Comput. Sci., 6: 199-204.

Zenzo, S.D., 1986. A note on gradient of a multi-image. Comput. Vison Graph. Image Process., 33: 116-125. DOI: 10.1016/0734-189X(86)90223-9